Efficient one-pot synthesis of monodisperse alkyl-terminated colloidal germanium nanocrystals

Darragh Carolan* and Hugh Doyle*

Tyndall National Institute, University College Cork, Lee Maltings, Cork, Ireland.

* Email: darragh.carolan@tyndall.ie

Email: hugh.doyle@tyndall.ie

Abstract: An efficient one-pot method for fabricating alkyl-capped germanium nanocrystals (Ge NCs) is reported. Ge NCs with a size of 3.9 ± 0.5 nm, are formed by co-reduction of germanium tetrachloride in the presence of n-butyltrichlorogermane, producing NCs with butyl terminated surfaces. The advantage of this method is that it allows rapid synthesis and functionalisation of NCs with minimal post-synthetic purification requirements. TEM imaging showed that the Ge NCs are monodisperse and highly crystalline, while EDX and SAED confirmed the chemical identity and crystal phase of the NCs. FTIR and XPS confirmed that the Ge NCs were well passivated, with some oxidation of the nanocrystal surface. Optical spectroscopy confirmed that the NCs were in the strong quantum confinement regime, with a strong absorbance in the UV region and an excitation wavelength dependent photoluminescence in the visible. Time resolved photoluminescence measurements showed the presence of two nanosecond lifetime components, consistent with recombination of photogenerated excitons at low lying energy states present at the nanocrystal surface. Photoluminescence quantum yields were determined to be 37 %, one of the highest values reported for organically terminated Ge NCs.

Germanium, nanocrystals, synthesis, photoluminescence, quantum yield

Introduction

In the last two decades semiconductor NCs have been the focus of intense research due to their size dependant optical and electrical properties (Rogach 2008; Schmid 2010). Much is now known about how to control their size, shape, composition and surface chemistry (Donega 2011; Gaponik et al. 2010; Linehan and Doyle 2014), allowing fine control of their photophysical and electronic properties, leading to utilisation in a range of applications from biological imaging to optoelectronic devices (Michalet et al. 2005; Talapin et al. 2009). However, genuine concerns have been raised regarding the toxicity of these II-VI and III-V materials, which contain heavy metals such as Cd, Pb and Hg (Bottrill and Green 2011; Council 2003; Ye et al. 2012; Winnik and Maysinger 2013). Germanium nanocrystals have recently attracted increasing attention as promising alternatives to II-VI and IV-VI semiconductor materials. As well as its high compatibility with current microelectronics, germanium is nontoxic, relatively inexpensive and biocompatible (Vaughn II and Schaak 2013). As a result, Ge NCs have lately been used in various applications such as biological imaging (Prabakar et al. 2010), field effect transistors (Holman et al. 2010) and hybrid photodetectors (Xue et al. 2011).

These applications not only require preparation of Ge NCs in high yield, but also with narrow size distributions and well characterised surface chemistries, as these

factors strongly influence Ge NC photophysical properties. A number of different solution phase synthetic approaches have been reported, including the metathesis reaction of $GeCl_4$ with Zintl salts (Taylor et al. 1999) and high temperature decomposition of organogermane precursors (Hoffman and Veinot 2012; Lu et al. 2005). Other methods include thermal co-reduction of amido based precursors (Gerung et al. 2005), aqueous phase reduction of GeO_2 powders by $NaBH_4$ (Wu et al. 2011), and other high temperature chemical reduction methods (Lee et al. 2009; Muthuswamy et al. 2012; Ruddy et al. 2010). Disadvantages associated with these methods include long reaction times, high temperatures and pressures, and extensive post synthetic purification procedures (Muthuswamy et al. 2012; Vaughn II and Schaak 2013).

One promising approach towards scalable preparation of size monodisperse Ge NCs is the reduction of germanium halides within inverse micelles. This approach, first reported by Wilcoxon et al. for the preparation of hydride terminated NCs (Wilcoxon et al. 2001), was later adapted using either thermally activated or Pt-catalysed hydrogermylation reactions to form alkyl- and amine-terminated NCs with covalent Ge-C surface bonds (Carolan and Doyle 2014; Fok et al. 2004; Prabakar et al. 2010). Despite the successes of the microemulsion synthetic approach for preparation of high quality, size monodisperse Ge NCs, the post synthetic purification remains lengthy, while the Pt catalyst used is toxic to cells (Wang et al. 2011).

To address these issues, we report an efficient one-step synthesis of Ge NCs with *in situ* passivation and straightforward purification steps. Ge NCs are formed by co-reduction of a mixture of germanium tetrachloride ($GeCl_4$) and n-butyltrichlorogermane; the latter is used both as a capping ligand and as a germanium source, see Scheme 1. When n-butyllithium is added, while the Ge-Cl bonds in both precursors are readily reduced, the Ge–C bond in n-butyltrichlorogermane is more stable, capping the surface and ultimately limiting the growth of the NCs. This surface-bound layer of butyl chains both chemically passivates the NC surface, providing protection against oxidation in ambient atmospheric conditions, and stabilises the Ge NCs to facilitate dispersal in a range of organic solvents.

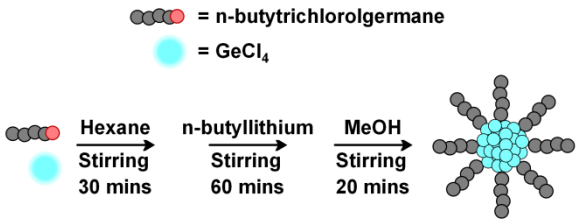

Scheme 1 Schematic of the one-pot method used to produce butyl terminated Ge NCs by co-reduction of $GeCl_4$ and n-butyltrichlorogermane by n-butyllithium.

Experimental Details

Synthesis and Purification of butyl terminated Ge NCs

Chemicals

Sulphuric acid (95-97%) and hydrogen peroxide (30% v/v) were purchased from Sigma Aldrich Ltd. and stored under ambient atmosphere. Germanium tetrachloride (99.99%), n-butyllithium (2.5M in hexanes), hexane (95%, anhydrous) and methanol (99.8%, anhydrous) were purchased from Sigma Aldrich Ltd. and stored under inert atmosphere before use. N-butyltrichlorogermane was purchased from Fluorochem Ltd. and stored under inert atmosphere before use. All materials and solvents were used as received.

Synthesis and Purification

All glassware used was cleaned by thoroughly soaking in a base bath overnight, followed by immersion in piranha solution (3:1 concentrated sulphuric acid: 30 % hydrogen peroxide) for 20 minutes. *CAUTION: Piranha solution is a strong oxidizing agent and should be handled with extreme care.* All synthetic manipulations were carried out in an inert atmosphere glove box with water and oxygen levels kept below 0.1 ppm in order to prevent simple hydrolysis of the Ge precursors. For Ge NCs prepared with both precursors, n-butyltrichlorogermane (142.7 µL) was added to hexane (60 mL), closely followed by $GeCl_4$ (100 µL) (1:1 ratio of precursors); for Ge NCs prepared with only one precursor, the same quantities (142.7 µL n-butyltrichlorogermane or 100 µL $GeCl_4$ in 60 mL hexane) were used. In all cases, the reaction mixture was stirred continuously for 30 minutes, followed by the drop wise addition of n-butyllithium (2 mL), which simultaneously reduces both germanium precursors to form n-butyl terminated Ge

NCs. Upon addition of the reducing agent, the clear solution turned a milky white colour. *CAUTION: germane gas, which is pyrophoric and highly toxic, could be evolved at this stage of the reaction and care should be taken to prevent exposure to air* (Wilcoxon et al. 2007). The solution was then left to stir for 1 h. The excess reducing agent was then quenched with the addition of methanol (40 mL) and left to stir for another 20 minutes, after which the reaction was stopped. The solution was then removed from the glove box and the organic solvent removed by rotary evaporation. The Ge NCs were then extracted into 20 mL of chloroform and sonicated for 10 min. The solution was first filtered using filter paper and filtered through PVDF membrane filters (Acrodisc, 0.2 μM). The Ge NCs were further purified by washing once with 20 mL deionised water (18.2 MΩ cm). Butyl-terminated Ge NCs remain in the chloroform phase.

Characterisation

Transmission Electron Microscopy

Transmission electron microscopy (TEM) images and selective area electron diffraction (SAED) patterns were acquired using a high-resolution JEOL 2100 electron microscope, equipped with a LaB_6 thermionic emission filament and Gatan DualVision 600 Charge-Coupled Device (CCD), operating at an accelerating voltage of 200 keV. TEM samples were prepared by depositing a 40 μL aliquot of the Ge NC dispersion onto a holey carbon-coated copper grid (300 mesh, #S147-3, Agar Scientific), which was allowed to evaporate under ambient conditions. Data for size distribution histograms was acquired by analysis of TEM images of exactly 200 NCs located at different regions of the grid. NC diameter was determined by manual inspection of the digital images; in the case of anisotropic structures, the diameter was determined using the longest axis. Energy Dispersive X-Ray (EDX) spectra were taken using an Oxford INCA x-sight detection spectrometer. Spectra were obtained from an area of the grid where there was a large amount of NCs. A process time of 3-4 seconds was used and the spectra obtained using an integration time of 40 s.

Optical Spectroscopy

Fourier Transform Infrared (FTIR) spectra were recorded on a Perkin Elmer Two spectrometer. Spectra were recorded on aliquots of Ge NCs in a liquid cell with

CaF_2 plates. UV-Vis absorption spectra were recorded using a Shimadzu UV PC-2401 spectrophotometer equipped with a 60 mm integrating sphere (ISR-240A, Shimadzu). Spectra were recorded at room temperature using a quartz cuvette (1 cm) and corrected for the solvent absorption. Photoluminescence (PL) spectra were recorded using an Agilent Cary Eclipse spectrophotometer. Quantum yields (QY) were measured using the comparative method described by Williams et al. (Williams et al. 1983). Dilute solutions of the Ge NCs in water were prepared with optical densities between 0.01-0.1 and compared against solutions of the reference emitter 9,10-diphenylanthracene in cyclohexane with similar optical densities. PL spectra of Ge NCs and reference solution were acquired using an excitation wavelength of 340 nm, and the total PL intensity integrated from 360-500 nm for both the NCs and reference emitter.

X-Ray Photoelectron Spectroscopy

X-ray photoelectron spectroscopy (XPS) measurements were carried out using a Kratos Ultra DLD photoelectron spectrometer. The narrow scan spectra were obtained under high vacuum conditions by using a monochromatic Al Kα x-ray radiation at 15 kV and 10 mA with an analyser pass energy of 20 eV. Substrates were cleaned for 20 min in piranha solution, rinsed with water and dried with a nitrogen gun. A few drops of the Ge NC dispersion dissolved in chloroform were dropped on a clean gold surface substrate. All spectra were acquired at room temperature and binding energies were referenced to the Au $4f_{7/2}$ line. All spectra were fitted with two peaks using a Shirley background.

Lifetimes

Photoluminescence lifetime measurements were recorded on a scanning confocal fluorescence microscope (MicroTime 200, PicoQuant GmbH) equipped with a TimeHarp 200 TCSPC board. NC samples were excited in solution using a 402 nm pulsed diode laser (10 MHz; 70 ps pulse duration, LDH-P-C-400) that was spectrally filtered using a 405 nm band-pass filter (Z405/10x, Chroma Technology Corp.). A 50X objective (0.5 NA; LM Plan FL, Olympus Corp.) was used for focusing the excitation light onto the NC dispersion and collecting the resultant fluorescence, which was directed onto an avalanche photodiode (APD; SPCM-AQR-14, Perkin-Elmer, Inc.). Backscattered excitation light was blocked

with a 410 nm long-pass filter placed in the collection path (3RD410LP, Omega Optical). The excitation power was adjusted to maintain a count rate of < 10^4 counts/s at the APD in order to preserve single photon counting statistics. All emission lifetimes were fitted to a weighted multi-exponential model on FluoFit 4.2 software (PicoQuant GmbH). All lifetimes were fitted with a χ^2 value of less than 1.1.

Results and Discussion

Fig. 1 shows a TEM image of the butyl capped Ge NCs formed by the reduction of $GeCl_4$ and n-butyltrichlorogermane. No aggregation of the NCs was observed and the size distribution of the NCs was determined to be 3.9 ± 0.5 nm from a count of 200 NCs, see the corresponding size histogram. Ge NCs formed by the reduction of only n-butyltrichlorogermane also showed narrow size distributions with a reduced diameter (3.4 ± 0.4 nm, see Fig. ESM1(a)), possibly due to the lesser amount of Ge precursor used in the synthesis. In contrast, Ge NCs prepared with an equivalent amount of $GeCl_4$ exhibited significant increases in both size and polydispersity, with an average diameter of 7.2 ± 0.6 nm, indicating that n-butyltrichlorogermane plays a role in regulating NC size and monodispersity, see Fig. ESM1(b).

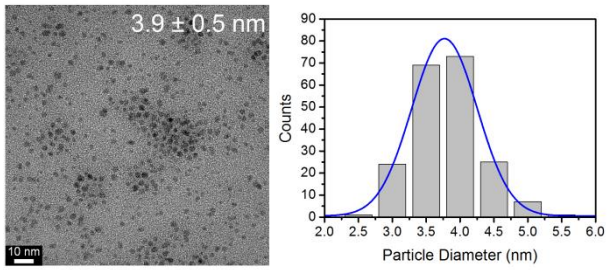

Fig. 1 Left, TEM image of Ge NCs synthesised by the reduction of both n-butyltrichlorogermane and $GeCl_4$. Right, histogram of Ge NC diameters fitted using a Gaussian model

High-resolution TEM (HR-TEM) imaging was used in conjunction with SAED to confirm the crystallinity and establish the phase of the NCs formed; see Fig. 2 (a) and (b). HR-TEM images (Fig. 2 (a)) showed that the Ge NCs form a single crystalline domain, with a lattice *d* spacing (2.0 Å) matching the (220) reflection of the germanium unit cell. The Fast Fourier Transform (FFT) of the HR-TEM image in Fig. 2(a), inset, exhibits the characteristic pattern of the diamond

germanium crystal structure, viewed down the [111] direction. SAED patterns of the Ge NCs (Fig. 2 (b)) showed reflections that could be indexed to Ge diamond cubic (*Fd3m*) lattice at 1; 3.3 Å (111), 2; 2.0 Å (220), 3; 1.7 Å (311), 4; 1.3 Å (331) and 5; 1.2 Å (422), respectively. EDX spectroscopy was employed to determine the elemental composition of the samples. Fig. 2 (c) shows an EDX spectrum recorded for the butyl capped Ge NCs. Characteristic Ge peaks were observed as well as Cu from the TEM grid support.

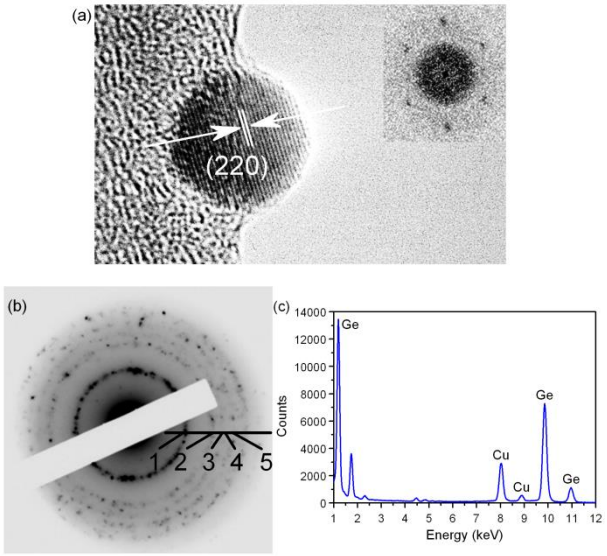

Fig. 2 (a) HR-TEM of an individual Ge NC, inset shows an FFT pattern, (b) SAED pattern for the Ge NCs and (c) EDX spectrum

The surface of the Ge NCs was characterised by FTIR and XPS spectroscopy, see Figs. ESM2 and ESM3, respectively. The peaks between 2855 and 2956 cm^{-1} are attributed to the CH_2 and CH_3 stretching modes of the alkyl group (Silverstein et al. 1991). The peaks at 1465 and 1260 cm^{-1} are ascribed to the scissoring and bending of the Ge-C and Ge-CH_2 bonds, respectively, while the strong peak at 1375 cm^{-1} is assigned to the C-CH_3 symmetric stretching mode (Carolan and Doyle 2014; Socrates 1980). The peak at 964 cm^{-1} is assigned to the Ge-O-Ge vibrations (Henderson et al. 2010), while the peaks below 900 cm^{-1} are a combination of the Ge-O and the Ge-C stretching modes (Taylor et al. 1999), consistent with a covalently attached alkyl layer with some surface oxidation. The XPS survey spectrum (Fig. ESM3(a)) shows no peaks due to the presence of Li or Cl from the reducing agent or precursor materials, while the Si2s and Si2p peaks between 150 to 100 eV are due to the substrate used in the measurement. The Ge3d spectrum (Fig. ESM3(b)) exhibits peaks at 30.5 and 32.2 eV, consistent

with a partially oxidised Ge NC surface. The O1s spectrum is fitted with two components at 532.3 and 533.9 eV, assigned to C-O and Ge-O bonds, respectively. The C1s XPS spectrum has a strong peak at 284.8 eV, assigned to C-C/C-H bonding, with a minor peak at 286.4 due to C-O bonds.

The optical properties of the butyl-terminated Ge NCs were investigated using UV-Vis absorbance, PL and photoluminescence excitation (PLE) spectroscopy; see Fig. 3(a). The UV-Vis spectrum shows a strong UV absorbance, with a small shoulder near 330 nm and an onset of absorbance at *ca.* 350 nm (3.5 eV), much higher in energy than the band gap of bulk Ge (0.6 eV). Similar spectral features have been previously reported in optical spectra of Ge NCs, (Wilcoxon et al. 2001; Ghosh et al. 2013) which were assigned to direct transitions from Γ_{25} to split energy levels at Γ_{15}; the significant blue shift in the onset of absorption compared to the bulk Ge band gap energy suggests the presence of quantum confined carriers in the nanocrystals. The PLE spectrum shows a narrow peak centred at *ca.* 290 nm (4.3 eV), considerably in excess of the observed onset of absorbance at 3.5 eV, with additional shoulders at 310 nm and 330 nm. The complex surface chemistry of the Ge NCs revealed by FTIR and XPS measurements, suggests the involvement of a number of different surface states in the photoluminescence process, although it is possible that radiationless transfer to lower lying energy states occurs prior to exciton recombination. The alkyl-terminated Ge NCs also exhibit a structured luminescence between 300-500 nm, with PL spectra clearly dependent on the excitation wavelength used, as the wavelength position of the PL maximum red-shifts from 358 nm to 433 nm as the excitation wavelength is increased from 290 nm to 400 nm, see Fig. 3(b). Increasing the excitation wavelength also results in a slight broadening of the PL spectrum (the full width at half maximum (FWHM)) increases from 72 nm to 91 nm) and a 10-fold decrease in the PL intensity as the excitation wavelength is increased. Ge NCs formed by the reduction of a single precursor show similar optical characteristics, see Fig. ESM4. While the UV-Vis absorbance of NCs prepared with n-butyltrichlorogermane is blue shifted with respect to the $GeCl_4$-derived NCs, which would be expected due to their smaller size, both NC samples possess similar structured PL spectra with a marked dependence on excitation wavelength.

As germanium is an indirect band gap semiconductor, optical transitions are allowed only if phonons are absorbed or emitted in order to conserve the crystal momentum. However, spatial confinement of electrons and holes inside a nanocrystal increases the uncertainty of their momentum, thus allowing optical transitions in which phonons are not involved. Due to the reduced number of energy levels and high surface to volume ratios inherent to semiconductor nanostructures, the chemical identity of surface states and the interface with the host matrix or environment must also be considered when describing their optical properties. The underlying mechanism for PL in Ge NCs is usually described either in terms of exciton recombination confined entirely within the nanocrystal core, or a surface chemistry model that emphasizes the importance of energy states at the NC surface (Carolan and Doyle 2014; Vaughn II and Schaak 2013; Dasog et al. 2013).

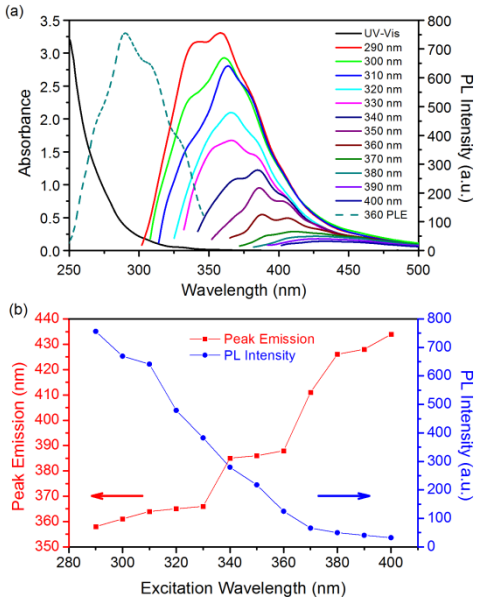

Fig. 3 (a) UV-Vis, PL and PLE spectra for Ge NCs in chloroform. (b) PL peak maximum (red squares) and intensity (blue circles) versus excitation wavelength

The PL spectra shown in Fig. 3(a) and ESM4 exhibit a structured blue emission that is independent of nanocrystal size, implying that exciton recombination is not confined within the nanocrystal core, does not involve Ge band states, and that nanocrystal surface states are involved in the emission process. The structured luminescence observed from Ge NCs (the normalized PL spectra are almost entirely superimposable) implies that a number of surface or near-interface states

are involved. This probably involves the oxygen-derived surface states (Ge-O_x and Ge-O-Ge) shown by FTIR and XPS, see Fig. ESM 2 and 3.

The excitation wavelength dependence of the PL could be attributed to sample polydispersity, with the larger NCs being selectively excited at longer wavelengths, but the narrow size distribution reported here rules out this explanation. Therefore, the origin of the excitation wavelength dependence is attributed to the involvement of different surface states in the luminescence process. Considering that the optimal excitation energies are considerably greater than the band gap energy, the sharp decrease in PL intensity at excitation wavelengths close to the absorption edge, the most plausible interpretation is that excitation at shorter wavelengths results in efficient generation of excitons, which readily transfer to and/or recombine at surface states to give blue emission. Excitation at longer wavelengths may result in less efficient generation of excitons, or increased transfer to non-radiative trap states, which would also contribute to the overall decrease in PL intensity.

The photoluminescence quantum yield (QY) of NCs prepared with both germanium precursors was determined using 9,10-diphenylanthracene as the reference emitter; see the ESM for further characterisation details. Fig. 4(a) shows the integrated PL intensities of dilute dispersions of the butyl-capped Ge NCs in chloroform and 9,10-diphenylanthracene in cyclohexane recorded under identical excitation conditions.

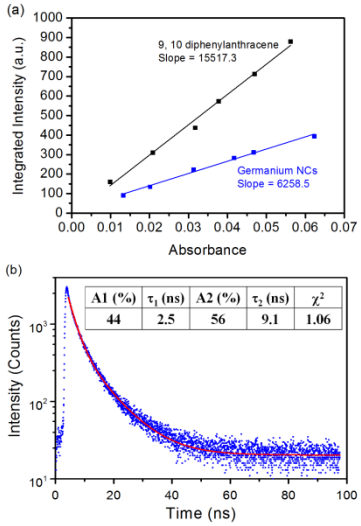

Fig. 4 Integrated PL intensity vs. absorbance for dilute dispersions of Ge NC in chloroform and 9,10-diphenylanthracene in cyclohexane. (b) PL decays of Ge NC dispersions. Inset: Table of fitted time constants and relative amplitudes

The QY of the Ge NCs was calculated to be 37 %, one of the highest reported to date for solution synthesised Ge NCs. PL lifetimes of the Ge NCs were acquired using time-correlated single photon counting methods (λ_{ex} = 402 nm); see Fig. 4(b). Measured transients were well fitted (χ^2 <1.1) to the sum of two weighted exponentials, yielding two lifetime components of 2.5 ns (44 %) and 9.1 ns (56 %), in line with previous reports (Shirahata et al. 2012; Warner and Tilley 2006). The nanosecond lifetimes observed provide further evidence that luminescence in Ge NCs is due to surface state recombination; band gap transitions in indirect semiconductors typically occur on microsecond timescales.

Conclusion

An efficient one-pot method for synthesis of size monodisperse, butyl-terminated Ge NCs with *in situ* surface passivation has been demonstrated. The advantage of this method is that it allows rapid synthesis and functionalisation of NCs with minimal post-synthetic purification requirements. TEM imaging showed that the NCs are monodisperse and highly crystalline, while EDX and SAED confirmed the chemical identity and crystal phase of the NCs. FTIR and XPS confirmed that the Ge NCs were well passivated, with some oxidation of the nanocrystal surface. Optical spectroscopy confirmed that the NCs were in the strong quantum confinement regime, with significant involvement of surface species in exciton recombination processes. Photoluminescence quantum yields were determined to be 37 %, one of the highest values reported for organically terminated Ge NCs.

Acknowledgements

This work was supported by the European Commission under the FP7 Projects HYSENS (grant agreement n° 263091) and CommonSense (grant agreement n° 261809) and the Irish Higher Education Authority under the PRTLI programs (Cycle 3 “Nanoscience” and Cycle 4 “INSPIRE”).

Electronic Supplementary Material (ESM) available: Additional TEM images, FTIR, XPS, optical spectra and determination of quantum yield.

References

Bottrill M, Green M (2011) Some aspects of quantum dot toxicity. Chem Commun 47:7039-7050 doi:10.1039/c1cc10692a

Carolan D, Doyle H (2014) Size and emission color tuning in the solution phase synthesis of highly luminescent germanium nanocrystals. J Mater Chem C 2:3562-3568 doi:10.1039/C4TC00319E

Council (2003) Directive 2002/95/EC on the restriction of the use of certain hazardous substances in electrical and electronic equipment. www.eur-lex.europa.eu.

Dasog M et al. (2013) Chemical insight into the origin of red and blue photoluminescense arising from freestanding silicon nanocrystals. ACS Nano 7:2676-2685 doi: 10.1021/nn4000644

Donega CdM (2011) Synthesis and properties of colloidal heteronanocrystals. Chem Soc Rev 40:1512-1546 doi:10.1039/C0CS00055H

Fok E, Shih ML, Meldrum A, Veinot JGC (2004) Preparation of alkyl-surface functionalized germanium quantum dots via thermally initiated hydrogermylation. Chem Commun:386-387 doi:10.1039/b314887d

Gaponik N, Hickey SG, Dorfs D, Rogach AL, Eychmüller A (2010) Progress in the light emission of colloidal semiconductor nanocrystals. Small 6:1364-1378 doi:10.1002/smll.200902006

Gerung H, Bunge SD, Boyle TJ, Brinker CJ, Han SM (2005) Anhydrous solution synthesis of germanium nanocrystals from the germanium(II) precursor Ge $[N(SiMe_3)_2]_2$. Chem Commun:1914-1916 doi:10.1039/b416066e

Ghosh B, Sakka Y, Shirahata N (2013) Efficient green-luminescent germanium nanocrystals. J Mater Chem 1:3747-3751 doi:10.1039/c3ta01246h

Henderson EJ, Seino M, Puzzo DP, Ozin GA (2010) Colloidally stable germanium nanocrystals for photonic applications. ACS Nano 4:7683-7691 doi:10.1021/nn102521k

Hoffman M, Veinot JGC (2012) Understanding the formation of elemental germanium by thermolysis of sol-gel derived organogermanium oxide polymers. Chem Mater 24:1283-1291 doi:10.1021/cm2035129

Holman ZC, Liu C-Y, Kortshagen UR (2010) Germanium and silicon nanocrystal thin-film field-effect transistors from solution. Nano Lett 10:2661-2666 doi:10.1021/nl101413d

Lee DC, Pietryga JM, Robel I, Werder DJ, Schaller RD, Klimov VI (2009) Colloidal synthesis of infrared-emitting germanium nanocrystals. J Am Chem Soc 131:3436-3437 doi:10.1021/ja809218s

Linehan K, Doyle H (2014) Size controlled synthesis of silicon nanocrystals using cationic surfactant templates. Small 10:584-590 doi:10.1002/smll.201301189

Lu XM, Korgel BA, Johnston KP (2005) Synthesis of germanium nanocrystals in high temperature supercritical CO_2. Nanotechnology 16:S389-S394 doi:10.1088/0957-4484/16/7/012

Michalet X et al. (2005) Quantum dots for live cells, in vivo imaging, and diagnostics. Science 307:538-544 doi:10.1126/science.1104274

Muthuswamy E, Iskandar AS, Amador MM, Kauzlarich SM (2012) Facile synthesis of germanium nanoparticles with size control: Microwave versus conventional heating. Chem Mater 25:1416-1422 doi:10.1021/cm302229b

Prabakar S, Shiohara A, Hanada S, Fujioka K, Yamamoto K, Tilley RD (2010) Size controlled synthesis of germanium nanocrystals by hydride reducing agents and their biological applications. Chem Mater 22:482-486 doi:10.1021/cm9030599

Rogach A (2008) Semiconductor nanocrystal quantum dots: Synthesis, assembly, spectroscopy and applications. Springer

Ruddy DA, Johnson JC, Smith ER, Neale NR (2010) Size and bandgap control in the solution-phase synthesis of near-infrared-emitting germanium nanocrystals. ACS Nano 4:7459-7466 doi:10.1021/nn102728u

Schmid G (2010) Nanoparticles: From theory to application. Wiley

Shirahata N, Hirakawa D, Masuda Y, Sakka Y (2012) Size-dependent color tuning of efficiently luminescent germanium nanoparticles. Langmuir 29:7401-7410 doi:10.1021/la303482s

Silverstein RM, Bassler GC, Morrill TC (1991) Spectrometric identification of organic compounds. Wiley, New York

Socrates G (1980) Infrared characteristic group frequencies. Wiley, Chichester

Talapin DV, Lee J-S, Kovalenko MV, Shevchenko EV (2009) Prospects of colloidal nanocrystals for electronic and optoelectronic applications. Chem Rev 110:389-458 doi:10.1021/cr900137k

Taylor BR, Kauzlarich SM, Delgado GR, Lee HWH (1999) Solution synthesis and characterization of quantum confined Ge nanoparticles. Chem Mater 11:2493-2500 doi:10.1021/cm990203q

Vaughn II DD, Schaak RE (2013) Synthesis, properties and applications of colloidal germanium and germanium-based nanomaterials. Chem Soc Rev 42:2861-2879 doi:10.1039/c2cs35364d

Wang J, Sun S, Peng F, Cao L, Sun L (2011) Efficient one-pot synthesis of highly photoluminescent alkyl-functionalised silicon nanocrystals. Chem Commun 47:4941-4943 doi:10.1039/c1cc10573f

Warner JH, Tilley RD (2006) Synthesis of water-soluble photoluminescent germanium nanocrystals. Nanotechnology 17:3745-3749 doi:10.1088/0957-4484/17/15/022

Wilcoxon JP, Provencio PP, Samara GA (2001) Synthesis and optical properties of colloidal germanium nanocrystals. Phys Rev B 64:035417 doi:03541710.1103/PhysRevB.64.035417

Wilcoxon JP, Provencio PP, Samara GA (2007) Synthesis and optical properties of colloidal germanium nanocrystals. Phys Rev B 76:199904 doi:19990410.1103/PhysRevB.76.199904

Williams ATR, Winfield SA, Miller JN (1983) Relative fluorescence quantum yields using a computer-controlled luminescence spectrometer. Analyst 108:1067-1071 doi:10.1039/an9830801067

Winnick FM, Maysinger D (2013) Quantum dot cytotoxicity and ways to reduce it. Acc Chem Res 46:672-680 doi: 10.1021/ar3000585

Wu J, Sun Y, Zou R, Song G, Chen Z, Wang C, Hu J (2011) One-step aqueous solution synthesis of Ge nanocrystals from GeO_2 powders. CrystEngComm 13:3674-3677 doi:10.1039/c1ce05191a

Xue D-J, Wang J-J, Wang Y-Q, Xin S, Guo Y-G, Wan L-J (2011) Facile synthesis of germanium nanocrystals and their application in organic-inorganic hybrid photodetectors. Adv Mater 23:3704-3707 doi:10.1002/adma.201101436

Ye L et al. (2012) A pilot study in non-human primates shows no adverse response to intravenous injection of quantum dots. Nature Nanotech 7:453-458 doi:10.1038/nnano.2012.74